Magnetic and magnetocaloric properties and the magnetic phase diagram of single-crystal dysprosium

A. S. Chernyshov,[1,2] A. O. Tsokol,[2] A. M. Tishin,[3] K. A. Gschneidner, Jr.,[1,2] and V. K. Pecharsky[1,2,*]
[1]*Department of Materials Science and Engineering, Iowa State University, Ames, Iowa 50011-2300, USA*
[2]*Materials and Engineering Physics Program,*
Ames Laboratory of the U.S. Department of Energy, Iowa State University, Ames, Iowa 50011-3020, USA
[3]*Department of Physics, M.V. Lomonosov Moscow State University, 119899 Moscow, Russia*
(Received 23 November 2004; published 23 May 2005)

Magnetic materials exhibiting magnetic phase transitions simultaneously with structural rearrangements of their crystalline lattices hold promise for numerous practical applications including magnetic refrigeration, magnetomechanical devices, and sensors. We undertook a detailed study of a single crystal of dysprosium metal, which is a classical example of a system where magnetic and crystallographic sublattices can be either coupled or decoupled from one another. Magnetocaloric effect, magnetization, ac magnetic susceptibility, and heat capacity of high-purity single crystals of dysprosium have been investigated over broad temperature and magnetic field intervals with the magnetic field vector parallel to either the *a* or *c* axes of the crystal. Notable differences in the behavior of the physical properties when compared to Dy samples studied in the past have been observed between 110 and 125 K, and between 178 and ~210 K. A plausible mechanism based on the formation of antiferromagnetic clusters in the impure Dy has been suggested in order to explain the reduction of the magnetocaloric effect in the vicinity of the Néel point of relatively impure samples. Experimental and theoretical investigations of the influence of commensurability effects on the magnetic phase diagram and the value of the magnetocaloric effect have been conducted. The presence of newly found anomalies in the physical properties has been considered as evidence of previously unreported states of Dy. The refined magnetic phase diagram of dysprosium with the magnetic field vector parallel to the *a* axis of a crystal has been constructed and discussed.

DOI: 10.1103/PhysRevB.71.184410 PACS number(s): 75.30.Sg, 71.20.Eh, 74.25.Ha

INTRODUCTION

The rare-earth metal dysprosium (Dy) has one of the largest magnetic moments in the lanthanide series, which for the free trivalent ion reaches $p_{eff}=g\sqrt{J(J+1)}=10.65\mu_B$, where g is the gyromagnetic factor, J is the total angular momentum quantum number, and μ_B is the Bohr magneton. In the ferromagnetically ordered state, the spontaneous magnetic moment of Dy is slightly lower, i.e., $m=gJ=10\mu_B$. The metal exhibits numerous magnetic phase transitions as temperature and/or magnetic field vary. In a zero magnetic field, Dy is in the paramagnetic (PM) state above its Néel temperature, $T_N\cong 180$ K. At ~180 K, elemental Dy transforms into a helical antiferromagnetic (AFM) phase, which is stable between ~90 and ~180 K. At the Curie temperature, $T_C\cong 90$ K, the metal orders ferromagnetically (FM) and remains in this state down to the lowest reported temperature of 4.2 K.[1–4] The transition between the AFM and FM phases at the Curie temperature is first-order, while that between the AFM and PM states at the Néel point is a second-order transformation. The intermediate fan magnetic structure emerges between the AFM and FM phases in a certain range of nonzero magnetic fields between ~127 and ~180 K.[4] A tricritical point on the phase diagram, where, in agreement with the Landau theory the nature of the AFM $\leftrightarrow$ fan transition changes from first to second order, is located near 165 K.[5]

In a zero magnetic field, the first-order phase transition from a helical AFM to a collinear FM state occurs simultaneously with the orthorhombic distortion of the hexagonal close-packed structure of the metal.[6] Above the Néel point, no short-range magnetic order has been observed by neutron scattering.[7,8] The x-ray diffraction investigation in low magnetic fields ($H\leqslant 1$ kOe), carried out in the vicinities of both the Curie and Néel temperatures, revealed a broad region where the AFM and FM phases coexist.[9] Kida *et al.*[10] reported similar observations in magnetic fields higher than 1 kOe. The crystallographic transition in Dy is preserved in nonzero magnetic fields, but according to Vorob'ev *et al.*,[9] the structural distortion is shifted to a higher temperature by ~3 K in a 1 kOe magnetic field when compared to that in a zero field. This result agrees with both the magnetization[4] and magnetocaloric effect (MCE) (Ref. 5) data.

Thermal expansion[11,12] and heat capacity[13] measured in a zero magnetic field reveal additional anomalies, such as steps and sudden slope changes, which were explained by temperature-dependent changes in the commensurability between the magnetic and crystallographic lattices. The correspondence between the anomalies and commensurability points was considered by Greenough *et al.*[14] with the objective to understand the nature of the complex temperature dependence of the thermal expansion and elastic constants in a zero magnetic field, and to relate the changes of the magnetic structure studied by neutron scattering with the elastic properties of Dy.

The investigation of the magnetization in magnetic fields ranging from 0 to 20 kOe applied along the hard magnetization direction, i.e., along the *c* axis of a crystal in a tempera-

ture interval from 4 to 300 K, was carried out by Jordan and Lee.[15] Magnetization, resistance, and thermal expansion studies conducted between 4 and 6.5 K enabled Wills and Ali[16,17] to conclude that a component of the magnetic moment along the *c* axis is likely present at low temperatures.

The magnetic phase diagram with the magnetic field applied along the *a* axis (the easy magnetization direction) has been constructed using different experimental methods. These include magnetization data,[4] ultrasonic measurements,[18] ac calorimetry,[13] magnetocaloric effect,[5,19] and Young's modulus.[19] Even though the magnetic and thermal properties of single crystalline Dy have been thoroughly studied, additional features in the magnetism and the need to revise the arrangement of phase fields in the vicinity of the Néel point were noted in Refs. 13, 20, 21, 22, and 23. Some of the anomalies can be explained by the occurrence of the intermediate vortex state, the presence of which in a narrow temperature range was predicted theoretically by Kosevich *et al.*[24] in the case of the magnetic field vector parallel to the *c* axis. As noted in Ref. 24, Dy—which is an easy plane magnetic material—may be unstable with respect to a transformation of the original magnetic phase into a vortex magnetic state perpendicular to the basal *ab* plane. Amitin *et al.*[25] suggested that the anomalous features of thermal expansion can be understood assuming the appearance of an intermediate vortex structure and by considering Dy as a two-dimensional magnetic system. The presence of the vortex state was experimentally verified by neutron scattering[7] in a zero magnetic field. The location of this additional magnetic phase on the *H*-*T* diagram with the magnetic field vector parallel to the $[11\bar{2}0]$ direction has been investigated by Alkhafaji and Ali[26] using magnetization measurements.

As mentioned above, the AFM$\leftrightarrow$PM magnetic transition in Dy is a second-order transformation, in agreement with the conventional theory of phase transformations. It is supported by the following experimental observations.

(i) The *H*-*T* diagram of Dy contains a tricritical point at $T=\sim 165$ K and $H=\sim 11$ kOe, where the first-order AFM$\leftrightarrow$FM (or AFM $\leftrightarrow$ fan) transition becomes a second-order transformation. Thus, at least the boundary of the AFM $\leftrightarrow$ fan transition approaches the zero magnetic field Néel point as a second-order transformation.

(ii) The AFM $\leftrightarrow$ fan transition takes place over a broad range of magnetic fields, and therefore has a continuous character.

(iii) The magnetic field hysteresis is absent in the range from the tricritical point ($\sim$165 K) to the Néel temperature (180 K).

Nevertheless, the presence of temperature hysteresis near the AFM$\leftrightarrow$PM phase transition, detected by heat capacity[13] and other properties[19] measurements, including magnetic field hysteresis of the magnetization in pulsed magnetic fields near the Néel temperature,[27] points to a mixed character of this phase transition. The presence of the extended temperature hysteresis in the paramagnetic region supports the notion about the existence of AFM clusters in the PM phase matrix. Both the amount and size of these clusters decrease with the increasing temperature, and the paramagnetic phase becomes uniform and homogeneous only at temperatures approximately 30 to 50 K above the Néel point.[19,28]

Since the behavior of the heat capacity at constant pressure, $C_p(H,T)$, as a function of temperature and magnetic field can be used to examine the nature of magnetic phase transitions, several sets of experimental investigations of the heat capacity of Dy have been reported to date. Specific heat was investigated by ac calorimetry from 80 to 130 K in a zero magnetic field[13] and in magnetic fields up to 17 kOe[19] applied along the easy magnetization direction (*a* axis). Unusual superheating during a first-order FM$\rightarrow$AFM transformation in a zero magnetic field was observed by Pecharsky *et al.*[29] and by Gschneidner *et al.*[30] for a solid-state electrolysis purified polycrystalline Dy.

The most recent magnetic phase diagrams of Dy (Refs. 13 and 26) indicate the presence of an unknown magnetic phase (the so-called "fan II" phase) inside the well-known fan phase region in the temperature interval from $\sim$170 K to $\sim$180 K and in magnetic fields between 12 and 25 kOe. The x-ray diffraction investigations[10] revealed anomalies of the temperature dependence of the *c* axis and thermal expansion in this region, but both of them can be explained without assuming the presence of an additional phase. Neutron-scattering data reveal differences in scattering between the conventional "fan" and the new fan II phases.[31]

In the past, the magnetic and thermal properties of single-crystal Dy were studied by various authors using different quality samples. The majority of known investigations were performed using specimens of different, often low, purity. Sometimes, impurities and their contents have not been quantified. Consequently, it is rather difficult to compare the results obtained by various authors in an attempt to develop a clear picture describing the nature of multiple phase transitions observed in elemental Dy as a function of temperature and magnetic field. To the best of our knowledge, a thorough investigation of the magnetothermal properties of this lanthanide metal employing a variety of experimental techniques with the magnetic field applied along different crystallographic directions in the same quality crystals obtained from a single initial batch of Dy was not conducted heretofore.

A comprehensive investigation of the magnetic and thermal properties of high-purity single crystals of Dy has considerable fundamental importance because the nature of magnetic phase transitions may be strongly affected in the total concentration of H, C, O, N, and/or F in the studied material exceeds a few hundred ppm by weight.[32] As we will show below, the magnetic phase diagram constructed using the results obtained from a high-purity Dy crystal contains several anomalous features and phases that were likely masked by interstitial impurities, and therefore left undetected in previous studies. Future theoretical investigations and neutron- and/or x-ray-scattering experiments should be conducted to gain a better understanding of the nature and behavior of the magnetic structure of Dy in these regions of temperature and magnetic fields. Such studies are especially important because it is also known that in low-purity single crystals of Dy, magnetic phase transitions have features typical of the coexisting first- and second-order phase transformations.[19]

In addition to furthering the basic understanding of the relationships between structure and magnetism, Dy may be

considered a classical example of a magnetic material where in certain regions of temperature and magnetic fields, a first-order magnetic phase transition coincides with a first-order structural transformation (in a zero magnetic field both transitions occur at ~90 K). Recent advancements in understanding complex intermetallic compounds[33] indicate that materials with combined magnetic-crystallographic transformations have a potential for practical applications, e.g., in energy-efficient and environmentally benign magnetic refrigeration. Presently, compounds with coupled magnetic and structural phase changes are believed to be the most promising class of materials[34–37] for future applications in magnetic cooling and heating.

In this paper, we report a variety of experimental measurements, including dc magnetization, ac magnetic susceptibility, magnetocaloric effect, and heat capacity, all as functions of temperature and magnetic field, performed using the identical quality Dy single crystals with magnetic field applied parallel to either the *a* or *c* axes of the crystal. The obtained results have been compared with previously known data and utilized in an attempt to explain the nature of the anomalies recently reported in Refs. 13 and 31.

EXPERIMENTAL DETAILS

The single crystal of Dy investigated in this work was prepared by the Materials Preparation Center at the Ames Laboratory. The major impurities in the polycrystalline metal used to grow the single crystal via a strain-anneal process were as follows (in ppm at.): O, 600; C, 190; F, 110; Fe, 60; and N, 50; thus the starting material was approximately 99.89 at. % (99.98 wt. %) pure. The specimens for the dc magnetization and ac magnetic susceptibility measurements were cut by using the spark-eroding technique from a large grain and shaped as parallelepipeds with the approximate dimensions $2\times2\times4$ mm^3. The longest axes of the parallelepipeds were parallel to either the *a*- or *c*-crystallographic axes of Dy. The samples for the heat capacity measurements, also extracted from a large grain, were approximately cylindrically shaped with the height of the cylinder around 3 mm, and its diameter approximately 10 mm; the *a*- and *c*-crystallographic axes were parallel to the shortest dimensions of the two different samples. Crystallographic directions were determined using the backreflection Laue technique. The combined accuracy of the alignment of the crystallographic axes with the direction of the magnetic field vector was $\pm5°$. All isothermal magnetization measurements reported in this paper have been corrected for demagnetization. The value of the demagnetization factor used for recalculating the magnetization was 0.2.

The dc magnetization and ac magnetic susceptibility data were measured using a Lake Shore ac/dc susceptometer/magnetometer, model 7225. Magnetic measurements were carried out in the range of external magnetic fields varying from 0 to 56 kOe and in the temperature interval from 4.5 to 300 K. The rms amplitudes of the ac magnetic fields varied from 2.5 to 10 Oe, and the range of the ac magnetic fields' frequencies was from 55 to 1000 Hz. The accuracy of the magnetic measurements, derived from measuring a Pt standard, appears to be better than 1%.

The heat capacity in constant magnetic fields ranging from 0 to 100 kOe was measured between ~4 and 350 K in a semiadiabatic heat pulse calorimeter, which has been described elsewhere.[38] The accuracy of the heat capacity data was better than ~0.6% in the temperature interval from 20 to 350 K and better than ~1% in the temperature range 4 –20 K.

The isothermal magnetic entropy change as a function of temperature was calculated from magnetization data by using the Maxwell relation

$$\Delta S_{mag}(T) = \int_0^H \left(\frac{\partial M}{\partial T}\right)_H dH. \tag{1}$$

The experimental isofield heat capacity data, $C_p(T,H_i)$ (usually a total of ~300 data points for each value of the external magnetic field), were used to calculate the total entropies, $S_{total}(T,H_i)$, where H_i is a fixed magnetic field,

$$S_{total}(T,H_i) = \int_0^T \frac{C_P(T,H_i)}{T} dT. \tag{2}$$

In Eq. (2), the zero-temperature entropy is assumed to be zero and independent of the magnetic field. In order to reduce the influence of a small variance in temperature at which the measurements in different H_i were initiated, the numerical integration of Eq. (2) was performed beginning at a common lowest temperature, $T_{\min}$, for all magnetic fields. Hence, the total entropy was calculated as follows:

$$S_{total}(T,H_i) = \int_0^{T_{\min}} \frac{C'_P(T,H_i)}{T} dT + \int_{T_{\min}}^T \frac{C_P(T,H_i)}{T} dT. \tag{3}$$

The heat capacity, $C'_P(T,H_i)$, was extrapolated from $T=T_{min}$ to $T=0$ using the experimental data in the temperature interval from ~3.5 to ~8 K and assuming that the total heat capacity is the sum of the lattice, electronic, and magnetic contributions. It was also assumed that at low temperature and faraway from the nearest magnetic phase transition ($T_C \equiv 90$ K), the contributions from the electronic (γT) and lattice (βT^3) heat capacities are magnetic-field-independent. Hence, magnetic field affects only the magnetic part of the heat capacity, $C_M = BT^n$, where $n=1.5$, and B is a parameter determined from a least-squares fit of the heat capacity data from T_{min} to ~8 K. Thus, the determined γ, B, and β were used in the interpolation from $T=T_{min}$ to $T=0$ K using $C'_P(T,H_i)=\gamma T+B_{Hi}T^{1.5}+\beta T^3$. The magnetocaloric effect was determined as the isothermal (ΔS_M) and the isentropic differences (ΔT_{ad}) between the two entropy functions: $S_{total}(T,H_i\neq0)$ and $S_{total}(T,H_i=0)$.

The magnetocaloric effect, ΔT_{ad}, was also measured directly from ~77 to 300 K in quasistatic magnetic fields using a home-built apparatus. The magnetic field changes ranged from 2 to 14 kOe and the magnetic field was generated by an electromagnet. Due to the relatively large magnetic induction of the coil, the time of the field sweep from 0 to 14 kOe was $\tau \cong 2$ s. The measurements were made on thermally insulated samples in a vacuum of $\sim10^{-3}$ torr to minimize the heat

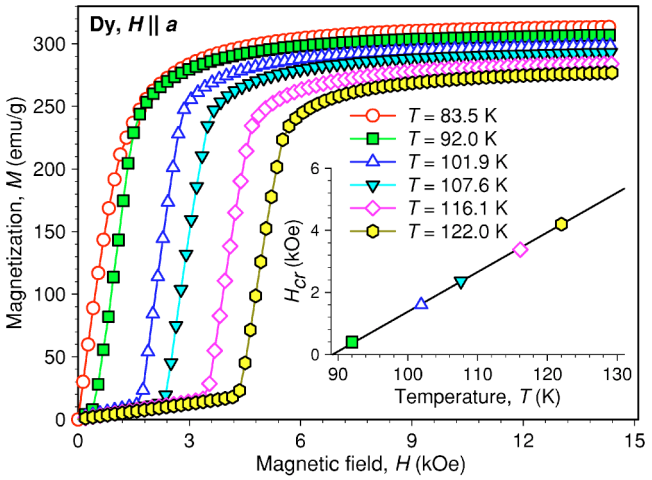

FIG. 1. (Color online) Isothermal magnetization of Dy measured between 83.5 and 122 K with the magnetic-field vector parallel to the *a* axis. The inset shows the critical magnetic fields as a function of temperature. The sample was heated to 250 K (i.e., the paramagnetic state) and then cooled down in a zero magnetic field to the temperature of each measurement.

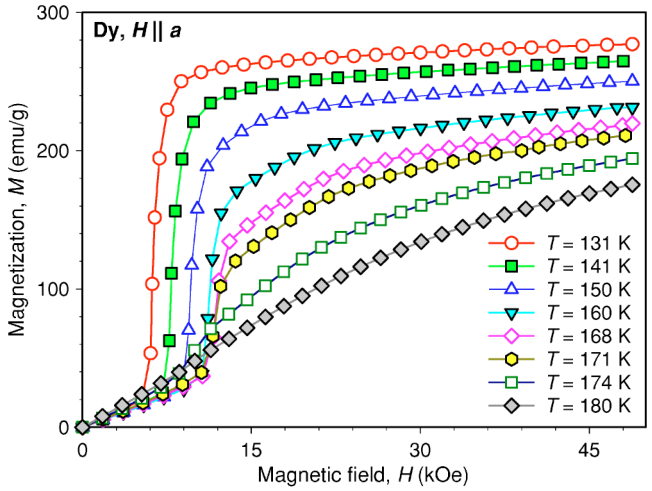

FIG. 2. (Color online) Isothermal magnetization of Dy measured between 135 and 180 K with the magnetic-field vector parallel to the *a* axis. The sample was heated to 250 K (i.e., the paramagnetic state) and then cooled down in a zero magnetic field to the temperature of each measurement.

exchange between the specimen and the surroundings. The MCE data were usually recorded as follows. First, the temperature of the specimen was stabilized after either cooling from ~200 K or heating from ~80 K to the target temperature in a zero magnetic field. Second, the MCE measurements were carried out by changing the magnetic field between zero and the desired value (and then back to zero) beginning from small magnetic field increments and ending with the largest ΔH. The zero-magnetic-field temperature of the specimen was kept constant during each series of measurements. We will refer to these data as the MCE measured isothermally. In another approach, which we call isofield measurements and which may yield different results because some phase transitions of Dy are first-order and hysteretic, the MCE data were recorded after sample temperature was stabilized as described above before each magnetic field sweep. The magnetic field change was always from zero to the same nonzero field value. The equilibrium temperature of the specimen was measured using a copper-constantan thermocouple before and after the magnetic field sweeps. The magnetocaloric effect was determined as the difference between the two equilibrium temperatures with ~7 to ~10% accuracy.

MAGNETIC PROPERTIES

The isothermal dependencies of the magnetization of the Dy single crystal measured in low magnetic fields in the temperature interval from 83.5 to 122 K with the magnetic field applied parallel to the *a* axis are shown in Fig. 1. Distinct metamagnetic-like steps in the magnetization corresponding to the magnetic-field-induced first-order AFM→FM transformation are observed at all temperatures exceeding 90 K. The critical magnetic field, H_{cr}, increases nearly linearly with temperature at a rate (dH_{cr}/dT) of 0.13 kOe/K, see inset in Fig. 1.

The magnetic field dependencies of the magnetization along the same crystallographic axis at higher temperatures and higher magnetic fields are shown in Fig. 2. The critical magnetic field required to induce the AFM→FM transformation continues to increase nearly linearly from ~4 to ~11 kOe with increasing temperature and then saturates at $H_{cr} \cong 11$ kOe at $T \geqslant 165$ K. A steplike increase in the magnetization is clearly observed even at 177 K (not shown in Fig. 2). At 180 K, the step becomes nearly indistinguishable and the anomaly is reduced to a change of slope of the $M(H)_T$ function, which presumably corresponds to a second-order magnetic-field-induced AFM ↔ fan transition. This behavior is in good agreement with the results reported in Ref. 2. In higher magnetic fields (11 to 22 kOe) and just below 180 K, Dy becomes ferromagnetic due to the magnetic-field-induced fan → FM transition. The magnetic-field-induced anomaly similar to that shown for the 180 K isotherm in Fig. 2 disappears above 181.5 K. The behavior of the magnetization becomes nearly linear with field as Dy adopts the paramagnetic state.

The magnetization along the *c* axis (Fig. 3) displays quite a different behavior, which is consistent with a hard magnetization direction. Between 120 and 180 K, anomalous but minor slope changes are observed in magnetic fields below 15 kOe. With increasing temperature, the location of this slope anomaly moves towards the higher values of the magnetic field in a nearly linear fashion.

The temperature dependencies of the magnetization along the *a* axis measured in several different dc magnetic fields are shown in Fig. 4. Sharp reductions of the magnetization observed on heating in 3, 6, and 10 kOe magnetic fields correspond to the temperature-induced first-order FM→AFM magnetic phase transitions. The cusps, seen near 180 K, correspond to second-order AFM→PM transitions. A weak anomaly is also observed in the vicinity of 100 K in low magnetic fields, which is better visualized as the derivative of the magnetization with respect to temperature (e.g., in

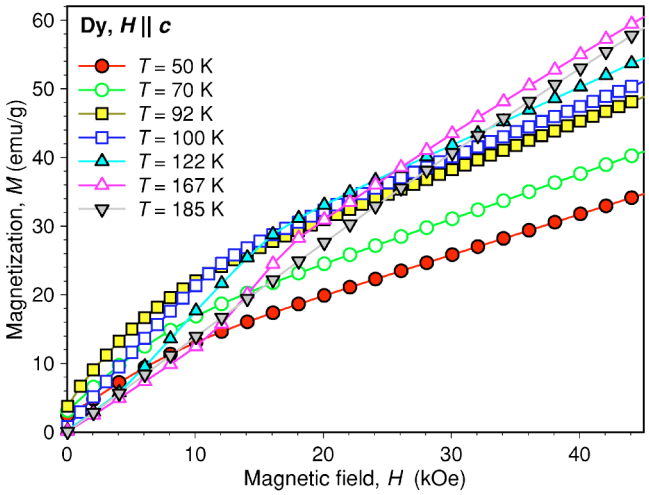

FIG. 3. (Color online) Isothermal magnetization of Dy measured between 50 and 185 K with the magnetic-field vector parallel to the *c* axis. The sample was heated to 250 K (i.e., the paramagnetic state) and then cooled down in a zero magnetic field to the temperature of each measurement.

a 6 kOe magnetic field, see inset in Fig. 4). The presence of the anomalies around 100 K may be explained by the proximity of the point where magnetic and crystal structures become commensurate with one another. Similar anomalies have been confirmed by our magnetocaloric effect measurements (see below), which also reveal the existence of an additional critical field in the temperature interval from 110 to 125 K.

The isofield magnetization measurements along the *c* axis in the temperature interval from 50 to 250 K and applied magnetic fields of 5 and 15 kOe are illustrated in Fig. 5. Both curves behave anomalously between 80 and 90 K (the Curie point) and around 180 K (the Néel point). The steplike decrease of the magnetization at ~80 reflects the first-order FM→AFM transition occurring on heating. The maximum of the magnetization at ~180 K coincides with the Néel point, where a second-order transition from the AFM to the PM phase occurs.

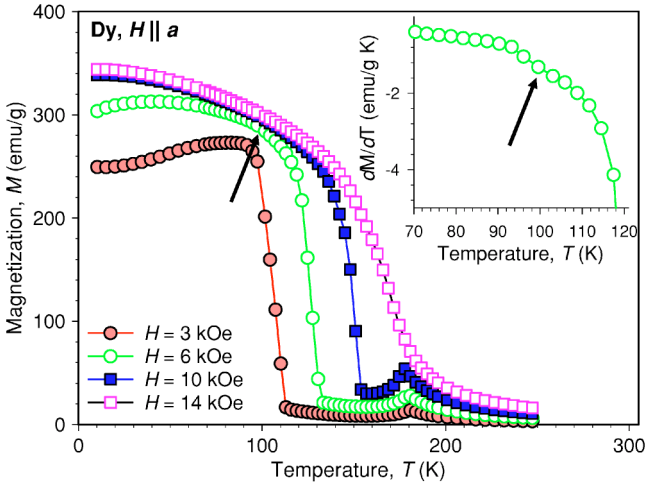

FIG. 4. (Color online) Isofield magnetization of Dy measured during heating of a zero magnetic field cooled sample from 4.5 to 250 K with the magnetic-field vector parallel to the *a* axis. The inset shows the derivative of the magnetization with respect to temperature between 70 and 120 K when $H=6$ kOe. The arrows point to a minor anomaly observed near 100 K in a 6 kOe magnetic field.

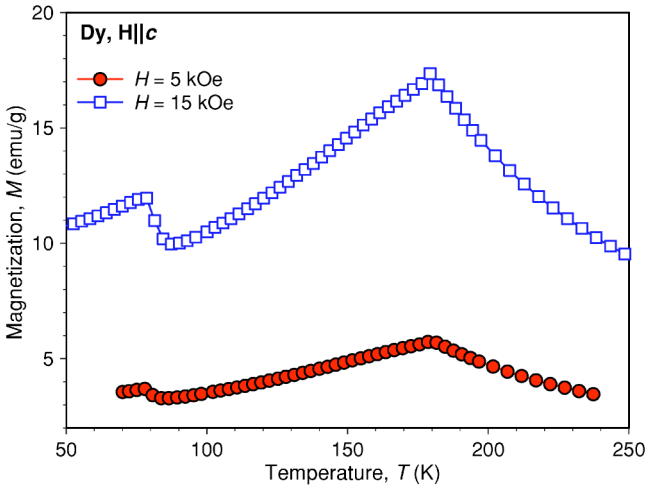

FIG. 5. (Color online) Isofield magnetization of Dy measured on heating of a zero magnetic field cooled sample from ~50 to ~250 K with a magnetic-field vector parallel to the *c* axis.

The temperature dependencies of the ac magnetic susceptibility measured along the easy magnetization axis with dc magnetic fields of 5 and 10 kOe applied along the *a* axis of the crystal are presented in Fig. 6. The anomalies observed when the sample was biased by a 5 kOe dc magnetic field (a minimum at 106.7 K, a maximum at 124.7 K, and a maximum at 180.2 K) correspond to the anomalies in the MCE (see below) and the dc magnetization (see Fig. 4) in this region of temperatures and magnetic fields. The minimum at 106.7 K is related to an intermediate magnetic phase. In the dc magnetic field of 10 kOe, the minimum of the ac susce-

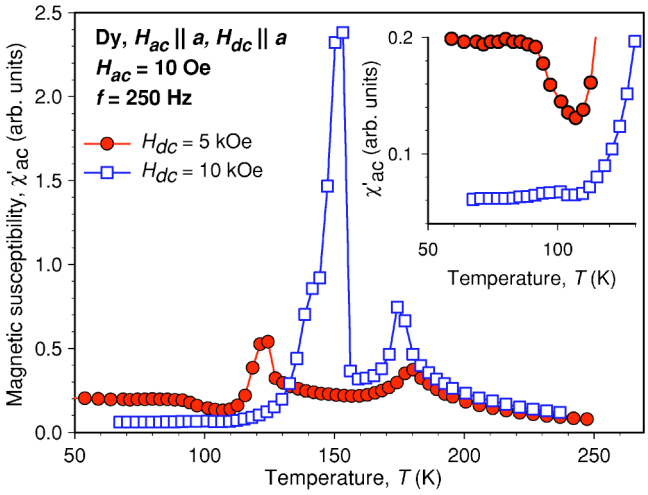

FIG. 6. (Color online) The real component of the ac magnetic susceptibility of Dy measured on heating of the zero magnetic field cooled sample from 50 to 250 K with both the ac and dc magnetic-field vectors parallel to the *a* axis. The inset clarifies details around 100 K.

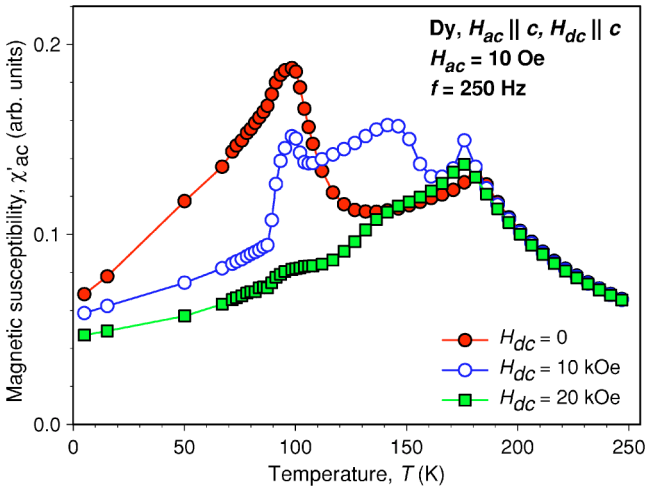

FIG. 7. (Color online) The real component of the ac magnetic susceptibility of Dy measured on heating of a zero magnetic field cooled sample from 5 to 250 K with both the ac and dc magnetic-field vectors parallel to the *c* axis.

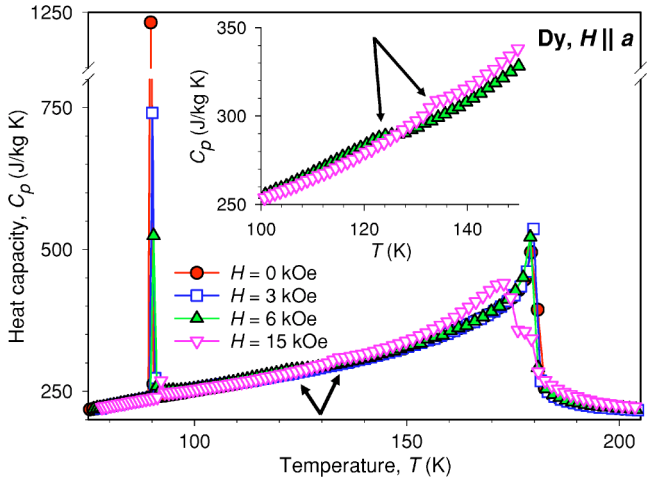

FIG. 8. (Color online) The heat capacity of Dy between ~70 and 250 K measured on heating of a zero field cooled sample in low magnetic fields with the magnetic-field vector parallel to the *a* axis. The inset clarifies the behavior between 100 and 150 K at 6 kOe and 15 kOe. The cusps, which develop in these magnetic fields, are indicated by arrows.

tibility transforms into a weak steplike anomaly (see inset in Fig. 6). There are also anomalies related to the second-order phase transition between ferromagnetic and fan phases ($T \cong 140$ K), the first-order AFM-FM magnetic phase transition ($T \cong 153$ K), and the second-order transition between AFM and PM phases ($T \cong 175$ K) when the ac susceptibility measurements are biased by a 10 kOe dc magnetic field.

The $\chi'_{ac}(T)$ data along the *c* axis measured in a zero external dc magnetic field have two peaks approximately corresponding to the locations of the Curie and Néel points (see Fig. 7). Additional steps appear in the applied dc magnetic fields of 5, 8, and 10 kOe (only the 10 kOe curve is shown in Fig. 7), and their locations on the temperature scale ascend in a linear fashion with the increasing magnetic field. In a 20 kOe magnetic field, the temperature dependence of the ac susceptibility has a characteristic maximum related to the position of the AFM↔PM transition and a step in the vicinity of the Curie temperature.

MAGNETOTHERMAL PROPERTIES

The heat capacity of single crystalline Dy in a zero magnetic field (see Fig. 8) agrees with the previous measurements.[13] A sharp peak at ~90 K corresponds to the first-order AFM→FM transition and the characteristic λ-type anomaly at ~180 K reflects a second-order AFM→PM transformation. Upon application of the magnetic field parallel to the easy magnetization direction, the behavior of the heat capacity changes considerably. The temperature of the sharp peak at 90 K remains nearly constant in magnetic fields between 3 and 15 kOe but its magnitude is gradually suppressed, especially in a 15 kOe field. The peak completely disappears in a 20 kOe magnetic field (not shown in Fig. 8). A second low-temperature feature—a small cusp—develops above 90 K in low magnetic fields, and it quickly shifts toward higher temperature as the magnetic field increases (see the inset in Fig. 8). The location of the cusp approximately corresponds to the magnetic-field-induced AFM→FM transitions (see Figs. 1 and 2). The high-temperature anomaly splits into two when the magnetic field is in the range of 15–25 kOe (only the 15 kOe data are shown in Fig. 8).

The heat capacity measured with the magnetic field applied along the *c* axis in the temperature interval 70 –200 K in the range of magnetic fields up to 15 kOe is shown in Fig. 9. Unlike when the magnetic field is applied parallel to the *a* axis, the data presented in Fig. 9 have only two anomalies. The sharp peak at ~90 K corresponds to a first-order phase transition. The magnitude of this peak decreases with increasing magnetic field, however the suppression is not as drastic as in the case when the magnetic field vector coincides with the easy magnetization direction. As long as the magnetic field is less than or equal to 20 kOe, its influence

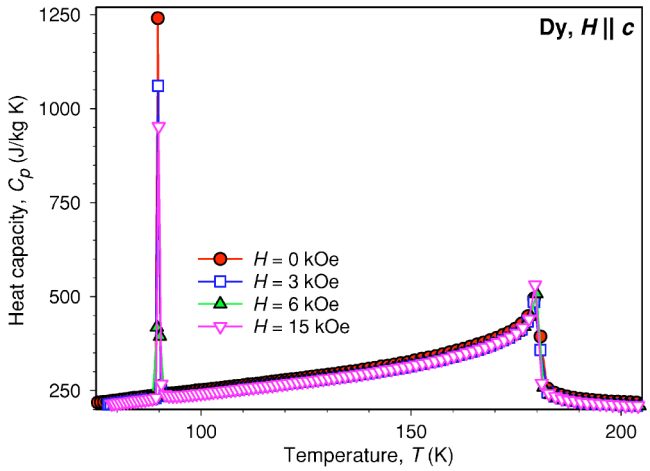

FIG. 9. (Color online) The heat capacity of Dy between ~70 and 250 K measured on heating of a zero field cooled sample in low magnetic fields with the magnetic-field vector parallel to the *c* axis.

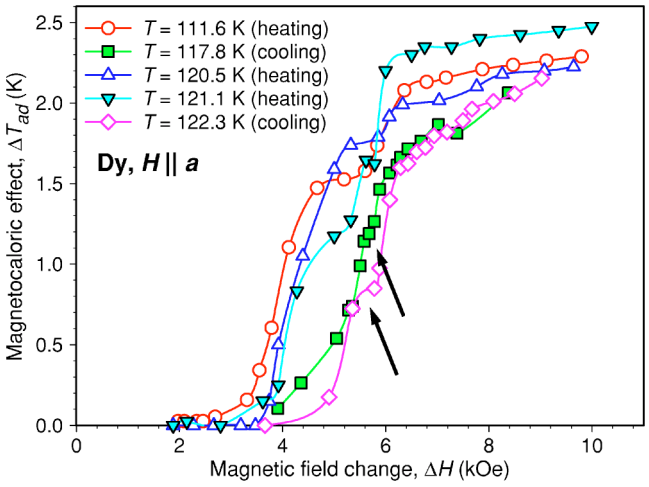

FIG. 10. (Color online) The magnetocaloric effect of Dy between ~111 and ~122 K measured directly in low magnetic fields with the magnetic-field vector parallel to the *a* axis. The magnetic field was changed between 0 and the value specified as the abscissa after the sample was either heated in a zero magnetic field from below 90 K or zero-field-cooled from above 180 K to the temperature of the measurement as indicated in the legend. The arrows point to low-field steps observed at $T=111.6$ and $T=117.8$ K.

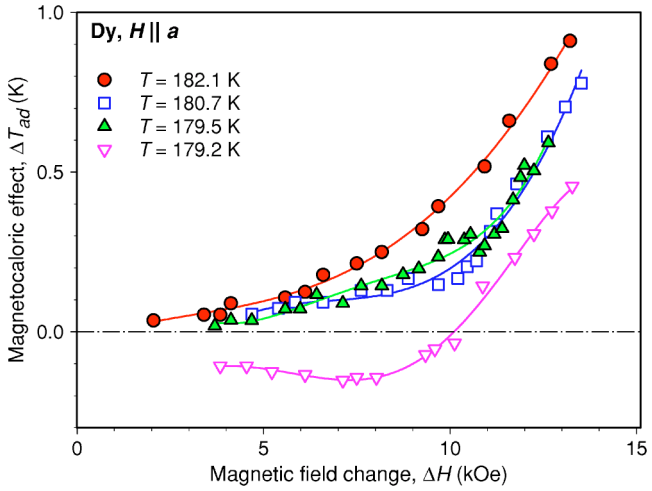

FIG. 11. (Color online) The magnetocaloric effect of Dy between ~179 and ~182 K measured directly in low magnetic fields with the magnetic-field vector parallel to the *a* axis. The magnetic field was changed between 0 and the value specified as the abscissa and then back to 0 while the sample was kept at constant initial temperature, as marked in the legend.

on the heat capacity around $T_N=180$ K is nearly negligible.

The isothermal dependencies of the magnetocaloric effect in the region from ~111 to ~122 K are presented in Fig. 10. Each curve displays two steplike anomalies. The low-field steps correspond to the magnetic-field-induced AFM→FM transitions. Additional steps occur at slightly larger magnetic fields and they are observed in the temperature interval from 105 to 125 K. The difference between the values of the critical fields corresponding to the first step, measured after heating and after cooling of the sample, shows temperature hysteresis, which is consistent with the first-order nature of the AFM→FM transition. The second steps have little, if any, hysteresis, thus indicating a second-order nature of the underlying transformation (also see below).

The isothermal behavior of the MCE in the vicinity of the Néel point is shown in Fig. 11. At and below 179.2 K, the MCE is negative in low magnetic fields, which is due to the contribution from the AFM phase in this range of magnetic fields. At higher temperatures, the antiferromagnetic order disappears, and the magnetocaloric effect becomes positive in all magnetic fields. It is, therefore, possible to define the Néel point as the temperature where the MCE becomes nonnegative in weak magnetic fields. The value of the thus obtained Néel temperature is 179.4 K. Just below the Néel temperature, the MCE shows a weakly magnetic-field-dependent plateaulike behavior (e.g., from ~4 to ~8 kOe at 179.2 K, from ~10 to ~12 kOe at 179.5 K, and from ~6 to ~8 kOe at 180.7 K). The fine features in the behavior of the MCE as a function of magnetic-field change disappear above 182 K, where Dy is in the PM state.

The temperature dependencies of the magnetocaloric effect for a magnetic-field change from 0 to 10 kOe between 50 and 200 K obtained using different techniques are depicted in Fig. 12. All of the data are presented without accounting for the demagnetization factor. Some discrepancies between the MCE values are observed in the temperature interval from 90 K to 160 K. The magnetocaloric effect measured isothermally generally exceeds that obtained from the isofield measurements, possibly due to the presence of an additional phase caused by the commensurability of the magnetic and crystallographic structures. The results computed from heat capacity are generally lower than those measured directly in this temperature range. While a variety of reasons may account for the discrepancies between the computed and the measured MCE values, including different error limits intrinsic to each technique,[39] we believe that the observed

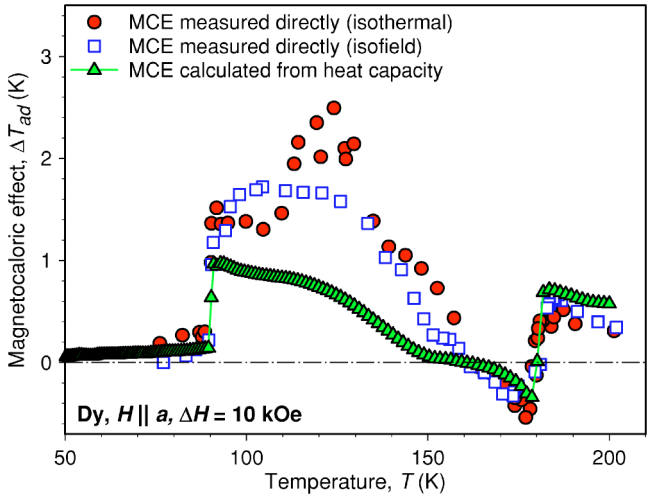

FIG. 12. (Color online) The magnetocaloric effect of single crystalline Dy between 50 and 200 K measured directly for a magnetic-field change from 0 to 10 kOe and calculated from the heat capacity data collected in 0 and 10 kOe magnetic fields. In all cases, the magnetic-field vector was parallel to the *a* axis of the crystal.

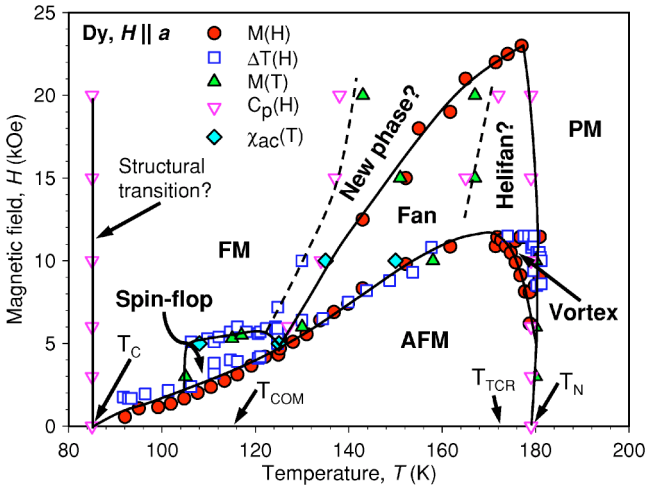

FIG. 13. (Color online) The magnetic phase diagram of Dy with the magnetic-field vector parallel to the easy magnetization direction, i.e., to the *a* axis of the crystal. Also see Figs. 17 and 20 for enlarged portions of the magnetic phase diagram in the range of 100 to 130 K and 3 to 7 kOe, and 170 to 180 K and 6 to 12 kOe, respectively.

differences are partially due to the fact that the heat capacity is measured in a constant magnetic field, while the direct MCE measurements require changing the magnetic field. Normally, this makes little, if any, difference unless the material undergoes a first-order phase transition, as does Dy, where the first-order AFM→FM transformation can be induced by low magnetic fields between 90 and ~180K (see Figs. 1 and 2).

All measured physical properties of Dy, especially those with the magnetic field parallel to the *a* axis of the crystal, show multiple temperature and magnetic-field-dependent anomalies. These are included in Fig. 13, which represents a refined *T-H* phase diagram of Dy. In general, most of the experimental results described in this section are in good agreement with those reported earlier. In particular, Dy behaves as a ferromagnet below the Curie temperature and as an antiferromagnet between the Curie and Néel temperatures in a zero magnetic field. We also detect anomalies, which can be associated with the intermediate fan phase during the transition from the AFM to FM phase when temperature exceeds ~125 K and the magnetic field exceeds ~4 kOe. At temperatures above 181.7 K, Dy behaves as a conventional paramagnet. Yet, several additional anomalies have been observed in the course of this study, thus leading to a revision of the magnetic phase diagram of Dy as discussed below.

AFM→FM PHASE TRANSITION

Magnetization and ac magnetic susceptibility measurements with the magnetic fields applied along the easy magnetization direction are in good agreement with previous investigations.[1–4] The Curie temperature is ~90 K in a zero magnetic field. As temperature increases, a small magnetic field is required to induce the AFM→FM transformation and the value of the critical magnetic field increases with temperature (see Fig. 13 and relevant experimental data in Fig. 1 through Fig. 7). Below the Curie temperature, magnetic and thermal properties indicate that the FM phase of Dy is in a uniform state.

The anomalous behavior of the heat capacity observed between 90 and 180 K when the magnetic field is applied along the *a* axis (Fig. 8) is related to complex interplay of magnetic and structural transitions between the AFM and FM phases. The lowest temperature anomaly is a sharp peak, which resides at ~90 K in magnetic fields up to 20 kOe. The second, next higher temperature anomaly, is a small cusp that in *T-H* coordinates (e.g., ~124 K at 6 kOe and ~135 K at 15 kOe) corresponds to the location of the magnetic-field-induced AFM→FM transition obtained from the magnetization data. It is, therefore, reasonable to assume that magnetic field applied along the easy magnetization direction leads to a two-step transformation in the elemental Dy. The first is the orthorhombic to hexagonal distortion, which appears to be magnetic-field-independent and always occurs at ~90 K on heating. In a nonzero magnetic field, this is likely to be a structural transition between two ferromagnetic phases of Dy. The second step is the *c*-axis discontinuity (according to Ref. 10 the discontinuity is observed at temperatures as high as 169 K), which is coupled with the FM→AFM change of the magnetic structure as temperature and field increase. Thus, the AFM↔FM transition in Dy involves an anisotropic change of the magnetoelastic interactions along the sixfold crystallographic axis,[19] and it appears that two structural (an orthorhombic - hexagonal distortion and the *c*-axis discontinuity) and one magnetic (AFM-FM) phase transitions coexist at T_C in a zero magnetic field. Thus, T_C may be considered as the lowest temperature tricritical point in the magnetic phase diagram of Dy.

Commensurability effects

The magnetocaloric effect data collected between 110 and 120 K reveal anomalous behavior of the isothermal MCE curves in the range of magnetic fields from 3 to 6 kOe (Fig. 10). Similar features have been observed in low magnetic fields in the thermal expansion at 100 and 110 K, and are thought to be caused by the proximity of the commensurability point at 113 K.[14] To gain further insights into the observed low magnetic field anomalies and to describe the behavior of the critical fields between ~110 and 120 K, one can employ the Landau-Ginsburg theory. Although the theory is phenomenological, it provides a qualitative understanding of the different magnetic phase transitions irrespective of their nature.

Theoretical analysis

Consider the helical antiferromagnetic structure of Dy (labeled "AFM" in Fig. 13) as a set of ferromagnetic planes stacked perpendicular to the *c* axis. From one plane to the next, the in-base components of the magnetic moments rotate by a specific angle φ, the so-called helix angle. According to neutron scattering,[14] the commensurability sets at T_{com} =113 K, in agreement with anomalies of the magnetic and thermal properties between 110 and 120 K described above.

At T_{com}, the nonzero c component of the magnetic wave vector $\mathbf{q}$ and the helix angle φ become, respectively, $1/6\tau$ and 30° (where τ is the length of the reciprocal-lattice vector). The magnetic moment, therefore, completes the full rotation over 12 sequential planes and one can consider these planes as an antiferromagnetic cluster consisting of six pairs of planes, each with mutually opposite magnetic moments. The investigation of how the commensurability point affects magnetic properties of a material was carried out in Refs. 40, 41, and 42. The case of a spiral structure with AFM ordering in the basal plane was described in Ref. 42.

For Ho and Dy, the Landau-Lifshitz function, expanded in the vicinity of the rational value of $\mathbf{q}=[0,0,1/6\tau]$, is as follows:[41]

$$\Phi = \frac{1}{V}\int d\mathbf{r}\left\{ r(\xi\eta) + u(\xi^2\eta^2) + w(\xi^6+\eta^6) + i\sigma\left(\eta\frac{d\xi}{dz} - \xi\frac{d\eta}{dz}\right) + \gamma\left(\frac{d\eta}{dz}\frac{d\xi}{dz}\right)\right\}. \tag{4}$$

In Eq. (4), ξ and η are the order parameters corresponding to clockwise and counterclockwise rotations of the magnetic moment in the basal plane, respectively; r, u, σ, and γ are the temperature-dependent coefficients; w represents the basal plane anisotropy; and V is the volume of a system. Equation (4) was obtained using full symmetry of the system at $\mathbf{q}=[0,0,1/6\tau]$.

The order parameters ξ and η represent a superposition of the left-handed and right-handed spirals. Therefore, the two variables can be reduced to one complex order parameter,[41]

$$\xi = \rho e^{i\varphi}, \quad \eta = \xi^* = \rho e^{-i\varphi}, \tag{5}$$

where ρ is the modulus (amplitude) of the order parameter. In the case of an undistorted helix structure of Dy, $\varphi=qz$, where $q=|\mathbf{q}|$ and z is the coordinate along the c axis.

After substituting the new variable into function (4), neglecting the fourth-order term, assuming that $\rho(\mathbf{r})$ is constant, and $\varphi(\mathbf{r})=\varphi(x,y,z)=\varphi(z)$ depends only on the z coordinate,[41] one can obtain the following simplified function:

$$\Phi = \frac{1}{V}\int d\mathbf{r}\left\{ r\rho^2 + \gamma\rho^2\left(\frac{d\varphi}{dz}\right)^2 + 2\sigma\rho^2\frac{d\varphi}{dz} + w\rho^6\cos 6\varphi\right\}. \tag{6}$$

Equation (6) does not account for the presence of 12-plane antiferromagnetic clusters caused by the commensurability of the crystal and magnetic structures of Dy. Thus, one must introduce an antiferromagnetic spiral, where the cluster is treated as an antiferromagnetically ordered slab. The density of magnetic moments inside the material in the case of the AFM spiral can be expressed as[42]

$$\mathbf{M}(\mathbf{r}) = M(\mathbf{m} + \mathbf{l}e^{-i\mathbf{q_A}r}), \tag{7}$$

where M is the modulus of the magnetization, $\mathbf{q_A}$ is the vector of the AFM structure inside the slab, and $\mathbf{m}$ and $\mathbf{l}$ are auxiliary vectors that satisfy the following conditions to keep the density of the magnetic moments independent of the coordinate:[42]

$$\mathbf{m}^2 + \mathbf{l}^2 = 1 \quad \text{and} \quad (\mathbf{m}\cdot\mathbf{l}) = 0. \tag{8}$$

If the magnetic field is applied along the easy magnetization a axis (x direction) and $\mathbf{q_A}$ is located along the c axis (z direction), then vectors $\mathbf{m}$ and $\mathbf{l}$ should have the following components:[42]

$$\begin{gathered} m_x = m\cos\varphi, \quad m_y = m\sin\varphi, \quad m_z = 0, \\ l_x = l\sin\varphi, \quad l_y = -l\cos\varphi, \quad l_z = 0, \end{gathered} \tag{9}$$

where $m=|\mathbf{m}|$ and $l=|\mathbf{l}|$ are the amplitudes of the vectors $\mathbf{m}$ and $\mathbf{l}$.

Considering the density of magnetic moments as the order parameter, one can obtain the function[42]

$$\frac{\Phi}{M^2} = \frac{1}{V}\int d\mathbf{r}\left[rl^2 + \gamma l^2\left(\frac{d\varphi}{dz}\right)^2 + 2\sigma l^2\frac{d\varphi}{dz} + mh\cos\varphi + wl^6\cos 6\varphi\right], \tag{10}$$

where l substitutes for ρ in Eq. (6).

Taking into account that $m^2+l^2=1$, minimization of the following equation models the phase transitions of the system:[42]

$$\frac{\Phi}{M^2} = \frac{1}{V}\int d\mathbf{r}\left[rl^2 + \gamma l^2\left(\frac{d\varphi}{dz}\right)^2 + 2\sigma l^2\frac{d\varphi}{dz} + mh\cos\varphi + wl^6\cos 6\varphi\right] - \lambda(m^2+l^2-1). \tag{11}$$

After differentiating Eq. (11) with respect to φ, l, m, and λ, one obtains the following series of Euler equations:

$$\begin{gathered} \frac{\delta(\Phi/M^2)}{\delta\varphi} = 0 \Rightarrow \frac{d^2\varphi}{dz^2} + \frac{mh}{2\gamma l^2}\sin\varphi + 6w\frac{l^4}{2\gamma}\sin 6\varphi = 0, \\ \frac{\delta(\Phi/M^2)}{\delta l} = 0 \Rightarrow l\left\{ r + \frac{1}{V}\int d\mathbf{r}\left[\gamma\left(\frac{d\varphi}{dz}\right)^2 + 2\sigma\frac{d\varphi}{dz} + 3wl^4\cos 6\varphi\right] - \lambda\right\} = 0, \\ \frac{\delta(\Phi/M^2)}{\delta m} = 0 \Rightarrow h\frac{1}{V}\int d\mathbf{r}\cos\varphi - 2m\lambda = 0, \\ \frac{\delta(\Phi/M^2)}{\delta\lambda} = 0 \Rightarrow m^2 + l^2 - 1 = 0, \end{gathered} \tag{12}$$

where l and m are treated as constants, and γ, σ, r, and w depend only on temperature.

Employing the perturbation theory for small values of the basal plane anisotropy (w) and taking into account only the terms that are linear with respect to w, we obtain the following approximate solutions for Eqs. (12):

$$\text{(I)}\ \phi = kz + \frac{w}{12\gamma}\sin 6kz, \quad l = 1,$$

$$m = 0 \ (h < h_2),$$

$$\text{(II) } \cos\phi = -1, \quad l = \sqrt{1-(h/2r)^2}, \quad m = -h/2r$$

$$(h_1 < h < h_3),$$

$$\text{(III) } \cos\phi = 1, \quad l = 0, \quad m = -1 \ (h > h_3),$$

$$\text{(IV) } \phi = 2\,\mathrm{am}\left(\sqrt{\frac{mh}{2\gamma l^2}}\frac{z}{\chi},\chi\right) + O\left(\frac{wl^{10}}{(mh)^3}\right), \quad m \cong 1, \quad l \ll 1 \ (h_2 < h < h_1), \tag{13}$$

where the limiting values of the magnetic field are

$$h_1 = 2|r|\left(\frac{16|r|}{\pi^2(\sigma^2/\gamma)} + 1\right)^{-1/2} + O(wl^2), \tag{14}$$

$$h_2 = \left[2\frac{\sigma^2}{\gamma}\left(\frac{\sigma^2}{\gamma} + |r| + O(w)\right)\right], \tag{15}$$

$$h_3 = 2|r|, \tag{16}$$

and the modulus χ of the amplitude of the Jacobian elliptic function, $\mathrm{am}(z/\chi,\chi)$, can be found by using the energy-conservation equation,

$$\frac{E}{\chi} = \left(\frac{1}{8}\pi^2(\sigma^2/\gamma)\frac{l^2}{mh}\right)^{1/2}, \quad E = \text{const}. \tag{17}$$

Solution (13.I) corresponds to a helix phase slightly distorted in the basal plane; solution (13.II) is an additional spin-flop phase that transforms to the ferromagnetic phase (13.III) when the magnetic field exceeds the critical value $h_3 = 2|r|$. Solution (13.IV) corresponds to a distorted helix. Relying on this phenomenological model, the region where the helix and the spin-flop phases coexist is defined in terms of the critical fields, i.e., when $h_2 > h_1$. Phase (13.IV), therefore, should not exist on the *H*-*T* phase diagram of Dy. As a result, the transition from the helix to the spin-flop phase is first-order, while that from the helix to the ferromagnetic state is a second-order transformation. After substituting these solutions into Eq. (11) and integrating over the volume of a sample, one can calculate the free energies,

$$\frac{\Phi_I(h,T)}{M^2} = -|r(T)| - \frac{\sigma^2(T)}{\gamma(T)},$$

$$\frac{\Phi_{II}(h,T)}{M^2} = -|r(T)|\left(1 - \left[\frac{h}{2|r(T)| + O(w)}\right]^2\right) - \frac{h^2}{2|r(T)| + O(w)}, \tag{18}$$

$$\frac{\Phi_{III}(h,T)}{M^2} = -h.$$

After comparing the free energies of different phases, the temperature dependencies of the critical magnetic fields related to the corresponding transitions are as follows:

$$h_{I\text{-}II} = h_{\text{H-SF}}(T) = 2\sqrt{|r(T)|[B(T) + O(w)]} \Rightarrow \quad \text{for helix} \rightarrow \text{spin-flop}, \tag{19}$$

$$h_{II\text{-}III} = h_{\text{SF-FM}}(T) = 2|r(T)| \Rightarrow \quad \text{for spin-flop} \rightarrow \text{FM}, \tag{20}$$

$$h_{I\text{-}III} = h_{\text{H-FM}}(T) = |r(T)| + B(T) + O(w) \Rightarrow \quad \text{for helix} \rightarrow \text{FM}. \tag{21}$$

In Eqs. (19)–(21), $B(T) = \sigma^2(T)/\gamma(T)$ is introduced for convenience only because the actual temperature dependencies of the coefficients r, σ, and γ are unknown.

Thus, the two boundaries of magnetic transitions $h_{\text{H-SF}}(T)$ and $h_{\text{SF-FM}}(T)$ may merge into a single $h_{\text{H-FM}}(T)$ line on the *T*-*H* magnetic phase diagram at a fixed temperature $T = T_{brn}$ (T_{brn} is the branching point at 127 K between spin-flop and FM states on the magnetic phase diagram of Fig. 13) and is defined by the condition

$$|r(T_{brn})| = B(T_{brn}) + O[w(T_{brn})]. \tag{22}$$

By differentiating the free energy of the system with respect to the magnetic field, one can obtain the temperature and field dependencies of the magnetization, M,

$$M(H,T) = \begin{cases} 0 & \text{if } H < h_{\text{H-SF}}M_S & \text{helix}, \\ \dfrac{H - 4\pi N M_S}{2|r(T)|} & \text{if } h_{\text{H-SF}}M_S < H < 2|r(T)| & \text{spin-flop}, \\ M_S & \text{if } H > 2|r(T)| & \text{FM}, \end{cases} \tag{23}$$

where M_S is the mean value of the magnetization and H is the value of the magnetic field.

To compare the experimental and theoretical curves of the MCE, we may use the magnetization calculated from Eq. (23) and the well-known expression for the MCE,

$$\Delta T = -\int_0^H \frac{T}{C_p}\left(\frac{dM}{dT}\right)dH, \tag{24}$$

where C_p is the heat capacity at constant pressure.

Comparison with the experiment

Using the experimentally determined temperature dependencies of the critical magnetic fields (see the magnetic phase diagram in Fig. 13), we first examine the correctness of our main assumption, i.e., that the basal plane anisotropy is small. The value of the basal plane anisotropy constant is $w = 0.04$ T g/emu (see Ref. 14). The average values of $|r| \approx h_{\text{H-SF}}/2 \cong 0.3$ T g/emu and $B \approx h_{\text{H-SF}} - |r| \cong 0.3$ T g/emu were estimated in the vicinity of the branching point $T_{brn} = 127$ K, where all the critical fields coincide and are approximately equal to $h_{\text{H-SF}} = 0.6$ T g/emu. We use the units of T g/emu to represent the basal plane anisotropy energy for convenience of the calculations. The corresponding ratios are, therefore,

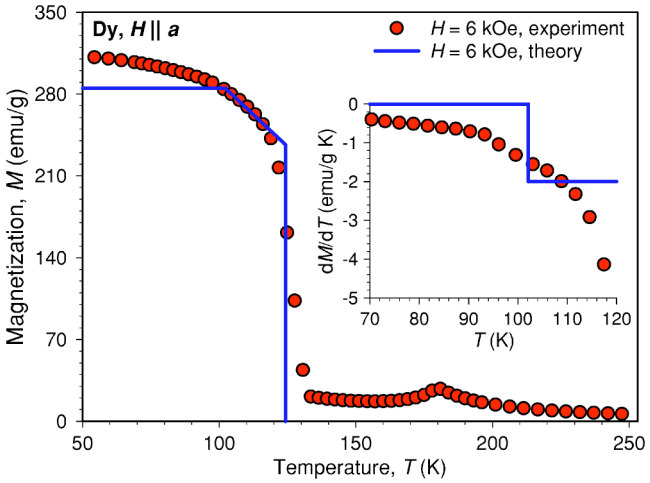

FIG. 14. (Color online) The temperature dependence of the magnetization measured along the *a* axis in the magnetic field of 6 kOe compared with calculated values [see Eq. (23)]. The inset shows the derivative of the magnetization with respect to temperature in the vicinity of the commensurability point.

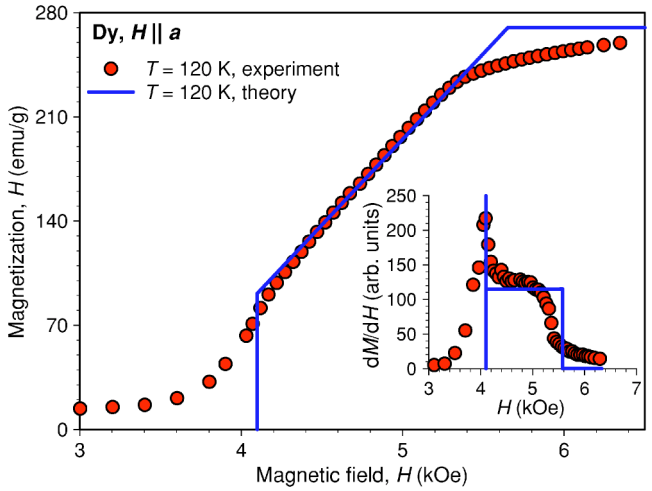

FIG. 15. (Color online) Magnetization of single-crystal Dy measured at 120 K between 3 and 6.4 kOe with the magnetic field applied along the *a* axis compared to that calculated using Eq. (23). The inset shows the derivative of the magnetization with respect to field.

$|w/r| \cong |w/B| \cong 0.1$, and in the first approximation, the basal plane anisotropy is indeed only a small perturbation.

The temperature dependence of the magnetization in a 6 kOe magnetic field is shown together with the theoretically predicted behavior in Fig. 14. The minor anomaly at ~100 K (better seen in the inset) corresponds to a second-order FM→ spin-flop phase transition. The distinct step around 123 K is associated with a first-order spin-flop →AFM transformation. The calculated $M(T)$ curve was determined from Eq. (23) by using the theoretically predicted temperature dependence of $|r(T)|$. The computed values of the magnetization were corrected for demagnetization factor, $N=0.15$, which is close to $N=0.2$ used to correct experimental data. The theory and experiment agree satisfactorily, facilitating calculations of the isothermal dependencies of the magnetization and MCE.

Another example comparing the measured and calculated [Eq. (23)] $M(H)_T$ is illustrated in Fig. 15. Two critical fields are seen at $T=120$ K. The first one corresponds to the inflection point during the jump of the magnetization around 4.1 kOe, and it manifests a first-order magnetic transition from a simple AFM spiral to a spin-flop phase. The second critical field (~5.6 kOe) is the change of slope due to a second-order phase transition from the spin-flop to the FM phase. Both features are seen as discontinuities of the derivative of the magnetization with respect to the magnetic field, as shown in the inset of Fig. 15, illustrating qualitative agreement between the experimental data and the model.

We also compare (Fig. 16) from Eqs. (23) and (24) the measured and calculated isothermal magnetic field dependencies of the MCE at $T=120$ K. In model calculations, the heat capacity at 120 K was taken to be magnetic-field-independent below 15 kOe, $C_p=278$ J/kg K (see Figs. 8 and 9). Once again, one can see a reasonable agreement between the theorymodel and the experiment. It is important to note that the anomalous MCE is both observed and reproduced theoretically in the temperature interval from 110 K to 130 K (see Figs. 10 and 12), i.e., where the simplification postulated above is applicable. The enhanced value of the magnetocaloric effect is, therefore, achieved due to the presence of the intermediate spin-flop phase.

Finally, in Fig. 17 we illustrate the part of the magnetic phase diagram between ~90 K and ~160 K with the magnetic fields under ~11 kOe applied along the easy magnetization axis. The experimental critical fields, obtained from magnetization, MCE, and ac magnetic susceptibility data are shown together with the second critical field boundary delineating the transition from the spin-flop to the FM state as calculated from the temperature dependence of the parameter $|r(T)|$. The agreement in this range of temperatures is nearly quantitative.

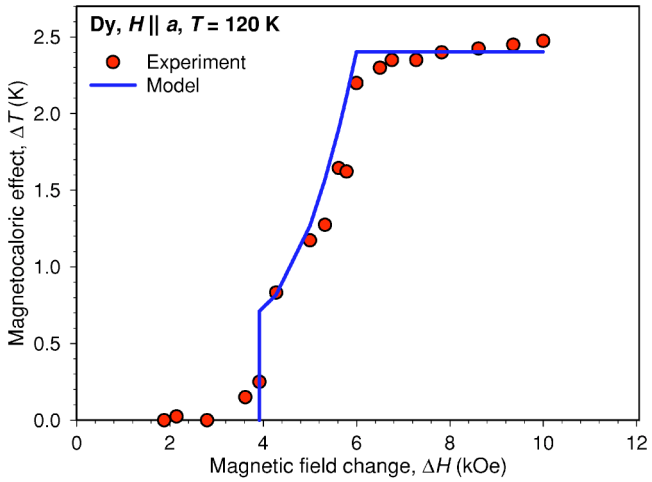

FIG. 16. (Color online) The comparison of the isothermal magnetocaloric effect of the single crystal of Dy at $T=120$ K measured experimentally with that predicted using Eqs. (23) and (24).

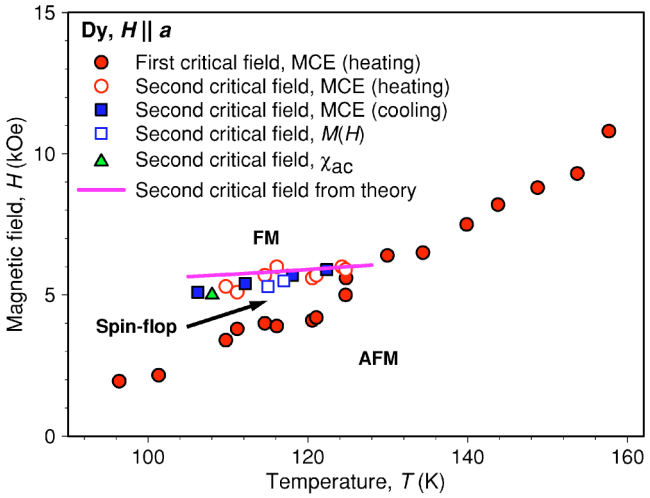

FIG. 17. (Color online) Details of the magnetic phase diagram of Dy with the magnetic field applied along the *a* axis in the vicinity of the commensurability point and the theoretically predicted boundary delineating the second critical field [see Eq. (20)].

The fan phase

An intermediate fan phase exists in the temperature interval from ~125 to ~180 K in the range of magnetic fields from ~5 to ~23 kOe when the magnetic field is applied along the easy magnetization direction (see Fig. 13). Its occurrence has been confirmed experimentally by using magnetization,[4] MCE,[5] ultrasonic measurements,[17] and a variety of other experimental data.[19] The theoretical discussion of the origin of the fan phase has been presented in Refs. 1 and 40. However, recent ac heat capacity[13] and neutron-scattering measurements[31] indicate that the assumed homogeneity of the fan phase region may not reflect reality. Our heat capacity data in this temperature-magnetic fields region (see Fig. 8) are in good agreement with the results,[13,31] and they confirm the presence of an additional phase between ~172 and ~180 K and between ~12 and 25 kOe. If one assumes similarity of Dy and Ho, it is possible to speculate that this additional phase is similar to the so-called "helifan" phase in Ho, theoretically predicted by Jensen and Mackintosh.[1] However, the corresponding calculations for Dy (Ref. 31) indicate that the helifan phase is unstable at any combination of temperature and magnetic fields.

Considering Kitano and Nagamiya's model described in Ref. 40, one can determine the temperature boundary of the region where the fan structure exists in a fixed magnetic field during the helix →fan→FM phase transitions. The magnetic field dependence of the fan angle φ at low temperatures can be written as[40]

$$\sin^2\frac{\varphi}{2} = \frac{2[J(\mathbf{q}) - J(0) - g_J\mu_B H/2S]}{[3J(\mathbf{q}) - 2J(0) - J(2\mathbf{q})]}, \tag{25}$$

where $J(\mathbf{q})$ is the Fourier transformation of the exchange integral $J(\mathbf{R}_{nm})$, the magnetic wave vector $\mathbf{q}$ is directed along the *c* axis, $J(0)$ is the value of $J(\mathbf{q})$ at the point $|\mathbf{q}|=0$, S is the total angular momentum quantum number of a magnetic atom, g_j is the Lande factor, and μ_B is the Bohr magneton.

The numerator of Eq. (25) is non-negative; it decreases with the increasing magnetic field and becomes zero at a fixed value of the magnetic field H_f, which corresponds to the fan →FM phase transition,

$$g_J\mu_B H_f = 2S[J(\mathbf{q}) - J(0)]. \tag{26}$$

It is worth noting that Eq. (26) does not explain the observed temperature dependence of the critical field. In order to do so, contributions from the basal plane anisotropy and the magnetoelastic interactions need to be considered.

For convenience, one can write the denominator of Eq. (25) in the following form:

$$3[J(\mathbf{q}) - J(0)] - [J(2\mathbf{q}) - J(0)]. \tag{27}$$

Since both the left-hand side and the numerator on the right-hand side of Eq. (25) are non-negative, the denominator on the right-hand side of this equation should be positive. Using the experimental data for $J(\mathbf{q})-J(0)$ from Ref. 1, one can analyze the sign of the denominator in order to establish the critical condition when the right-hand side becomes negative and Eq. (25) is no longer valid. As a result, there should be a certain value of the magnetic wave vector, q_{cr}, where for any values of q exceeding q_{cr}, the conventional fan structure does not exist. Taking into account the almost linearly increasing temperature dependence of the magnetic wave vector obtained from neutron-scattering measurements,[31] it is possible to estimate the critical temperature as $T_{cr}=172$ K corresponding to the value of q_{cr}. Hence, at temperatures exceeding T_{cr}, the fan should disappear in any magnetic field.

The estimates mentioned above are in support of the experimentally established configuration of the magnetic phase diagram of Dy illustrated in Fig. 13. As will be shown below, the critical temperature $T_{cr}=172$ K also coincides with the location of the experimentally observed tricritical point $T_{tcr}=172$ K and $H_{tcr}=11.2$ kOe.

We now discuss some differences in the behavior of the magnetization and heat capacity as functions of temperature. The heat capacity exhibits a maximum at $T\cong 171$ K and a slope anomaly at ~180 K in both 15 kOe (Fig. 8) and 20 kOe magnetic fields. The magnetization, however, displays inflection at ~170 K but has no obvious anomalies around 180 K in magnetic fields of 15 kOe (see Fig. 4 illustrating the same for the nearly identical field of 14 kOe) and 20 kOe. This discrepancy leads to an uncertainty in the location of the Néel temperature in nonzero magnetic fields.

Taking into account the model of the AFM fan structure of Dy described above, it is easy to realize that both the magnetization and heat capacity should reflect the changes that may occur within the fan as both the magnetic field and temperature vary. Thus, it is possible to assume that the typical paramagnetic dependence of the magnetization following an inflection point in low magnetic fields indicates weakened correlations between the ferromagnetic planes above $T_{cr}=172$ K. In fact, Dy may become a "two-dimensional paramagnet," where the orientations of the ferromagnetically ordered moments of one plane are only weakly correlated with those in the neighboring plane. At the Néel point, which coincides with the inflection point on the temperature dependence of heat capacity, the in-plane ferromagnetic order is

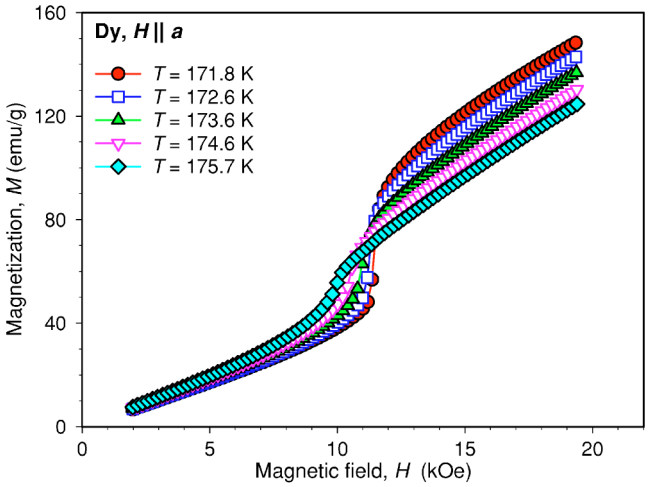

FIG. 18. (Color online) The isothermal dependencies of magnetization of a single crystal of Dy measured between 171.8 and 175.7 K with the magnetic-field vector parallel to the *a* axis of the crystal.

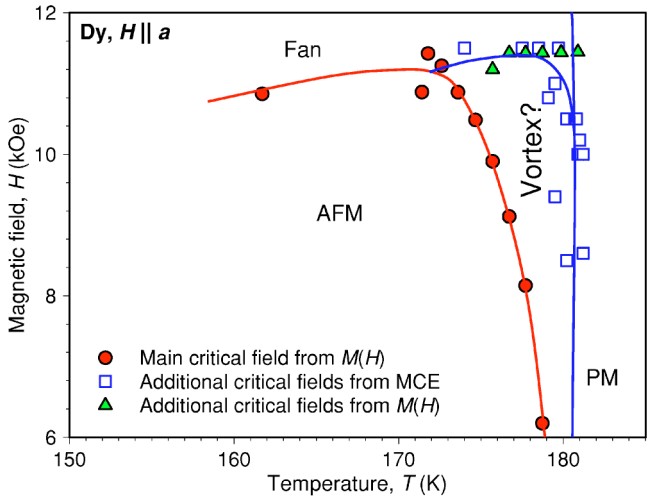

FIG. 20. (Color online) Details of the magnetic phase diagram of Dy with the magnetic field applied along the *a* axis in the vicinity of the Néel point.

destroyed and Dy becomes a conventional three-dimensional paramagnet. Thus, in the range of magnetic fields between 15 and 20 kOe, the Néel temperature cannot be obtained from magnetization data, and it probably should be defined from the location of an inflection point on the temperature dependence of the heat capacity. This interpretation, however, requires further experimental and theoretical study.

The vicinity of Néel and tricritical points

In order to refine the magnetic phase diagram near the Néel point, we performed detailed low-field isothermal measurements of the magnetization between 172 and 181 K. These data are shown in Figs. 18 and 19. As noted earlier, the sharp, nearly discontinuous M vs H behavior is seen at temperatures as high as 174 K. Between ~175 and ~181 K, the discontinuity evolves into an inflection point and the latter disappears at $T_N = \sim 181$ K. The anomalies of $M(H)$ at temperatures closest to the Néel point are better seen on the plots of $[\partial M(H,T)/dH]_T$, shown in the inset of Fig. 19. At $T = 178.7$ K, the first peak at 6 kOe corresponds to a second-order AFM → intermediate phase transition. The anomaly around 11.5 kOe at the same temperature manifests a second inflection point of $M(H)$ corresponding to a field-induced transition from the intermediate phase region into the fan phase.

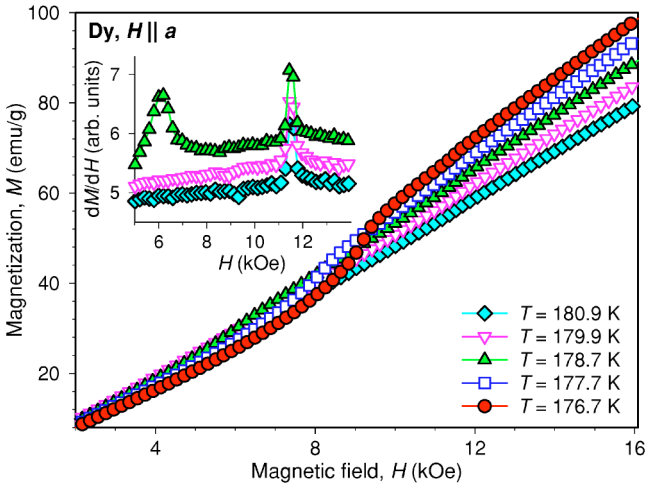

FIG. 19. (Color online) The isothermal dependencies of magnetization of a single crystal of Dy measured between 176.7 and 181.9 K with the magnetic-field vector parallel to the *a* axis of the crystal. The inset shows the derivatives of the magnetization with respect to magnetic field at temperatures close to the Néel point.

A detailed view of the magnetic phase diagram of Dy with the magnetic field applied along the easy magnetization axis in the vicinity of Néel temperature is shown in Fig. 20 The intermediate phase exists around 180 K in the range of magnetic fields from ~6 kOe or lower to ~12 kOe. The critical fields obtained from the magnetization (see Fig. 18 and Fig. 19) and direct MCE measurements (see Fig. 11) are in satisfactory agreement with one another. A similar intermediate phase region has been reported recently by Alkhafaji and Ali,[26] who used magnetization measurements with the magnetic field applied along the $[11\bar{2}0]$ direction. The appearance of the intermediate phase in the vicinity of the Néel temperature can be explained by the presence of the so-called "vortex" state. The formation of the vortex phase with the magnetic field applied along the *c* axis of a crystal was theoretically investigated by Kosevich *et al.*,[24] who also showed that the vortex state may even occur in a zero magnetic field.

Impurity effects

Clarifying how the purity of a specimen affects the value of the paramagnetic Curie temperature, θ_p, and the location of the tricritical point, T_{tcr}, on a magnetic phase diagram poses an interesting basic question, especially because of the presence of the intermediate vortex state phase. The tricritical point is a point along a phase boundary where a first-order transition evolves into a second-order transformation.

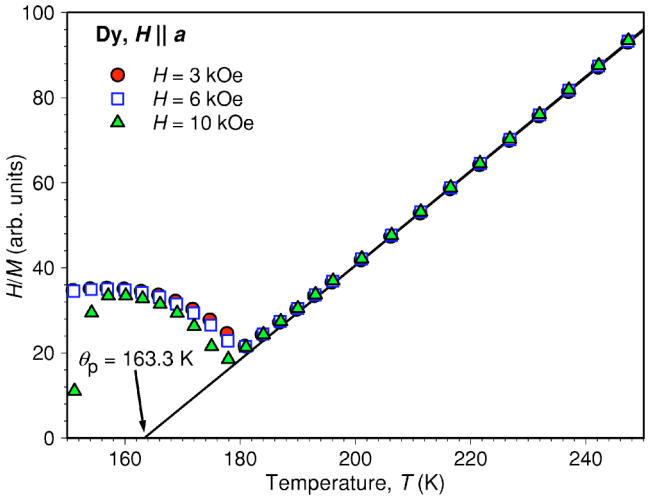

FIG. 21. (Color online) The inverse magnetic susceptibility of Dy measured in different magnetic fields. The lines correspond to the Curie-Weiss fit of the data above ~210 K.

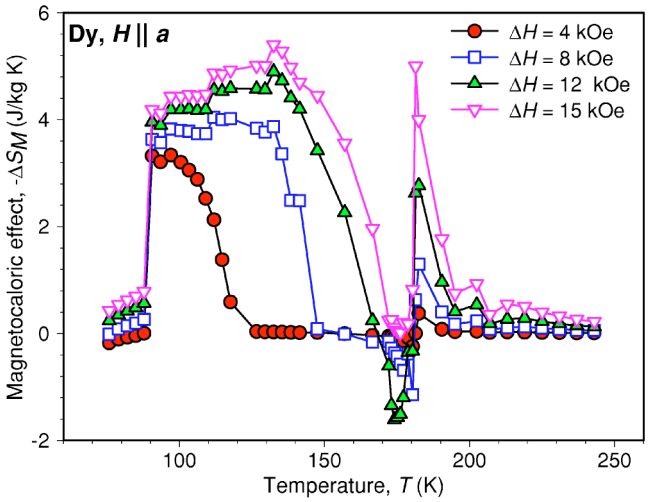

FIG. 22. (Color online) The temperature dependencies of the low-field isothermal magnetic entropy change calculated from the magnetization data in the temperature interval from ~70 to ~250 K.

The value of dH_{cr}/dT should be equal to zero at $T=T_{tcr}$. As follows from our magnetization measurements (see Fig. 18 and Fig. 20), T_{tcr} of pure Dy is 172 K. This value is higher than the 165 K reported in Refs. 4, 5, and 19, where the purity of Dy was lower. Also, as easily seen from the Curie-Weiss behavior illustrated in Fig. 21, the higher the purity of Dy, the higher its paramagnetic Curie temperature: we obtain $\theta_p=163.3$ K, while the values listed in Refs. 1, 19, and 40 are lower by several degrees Kelvin, i.e., $\theta_p=159$ K.

We now recall several expressions proposed by Kitano and Nagamiya (see Ref. 40) in order to describe the sequence of helix →fan→FM transitions of Dy. The first equation relates Néel and tricritical point temperature,

$$\frac{T_N - T_{tcr}}{T_N} \cong \frac{8}{11}\frac{J(\mathbf{q}) - J(0)}{2J(\mathbf{q})}, \tag{28}$$

where $J(\mathbf{q})$ is the Fourier transformation of the exchange integral $J(\mathbf{R}_{nm})$, vector $\mathbf{q}$ is directed along the c axis, and $J(0)$ is the value of $J(\mathbf{q})$ at $\mathbf{q}=0$ and $T_N=181$ K. The next two define, respectively, the Néel and paramagnetic Curie temperatures as follows:[40]

$$T_N = 2J(\mathbf{q})\frac{S(S+1)}{3k_B}, \tag{29}$$

$$\theta_p = 2J(0)\frac{S(S+1)}{3k_B}, \tag{30}$$

where S is the total angular momentum quantum number and k_B is the Boltzmann constant. Using Eqs. (28)–(30) and the experimentally determined $\theta_p=163.5$ K, the location of the tricritical point should be

$$T_{tcr} = T_N\left[1 - \frac{8}{11}\frac{T_N - \theta_p}{T_N}\right] \cong 168.4 \text{ K}. \tag{31}$$

The theoretically predicted 168.4 K is lower that $T_{tcr}=172$ K observed experimentally in a high-purity single crystal but it exceeds the 165 K reported for lower-purity specimens. The temperature difference between the T_{tcr} and T_N in a relatively pure Dy used in our study is 9 K, which is smaller by about 3 K than the difference between the same temperatures in a less pure metal. Therefore, it is possible to speculate that as the material's purity improves, the tricritical point may approach T_N. If this assumption is correct, then some of the phase fields in this part of the magnetic phase diagram of Dy may have a different configuration, or there may be even fewer phase fields on the diagram. In the limiting case, the AFM-fan boundary may approach the nearly vertical AFM-PM boundary with zero dH_{cr}/dT. Hence, the point where these boundaries meet becomes a tricritical point. Therefore, it is quite possible that the range where the vortex and other unknown phases were observed near T_N will become much narrower or even disappear in a much higher-purity Dy sample.

Magnetocaloric effect

The temperature dependencies of the isothermal magnetic entropy change, ΔS_M, in the temperature interval from ~70 to ~250 K with the magnetic field applied along the easy magnetization direction in the range of magnetic field changes from 0 to 4, 8, 12, and 15 kOe are shown in Fig. 22. The ΔS_M in the temperature interval from ~4 to 300 K for much larger magnetic field changes, i.e., from 0 to 20, 50, 75, and 100 kOe, is illustrated in Fig. 23. Several features seen in the behavior of the MCE are worth mentioning. First, the discontinuity of $\Delta S_M(T,\Delta H)$ at ~90 K remains independent of both T and ΔH, although the "background" contribution to the MCE below and above 90 K continues to increase as the magnetic field change increases. This behavior of the magnetocaloric effect is typical of first-order phase-transition materials and it has been predicted by Pecharsky *et al.*[43] Second, the amplitude of the MCE discontinuity at ~90 K, $\delta(\Delta S_M)=0.55$ J/mol K (see Figs. 22 and 23), is in excellent

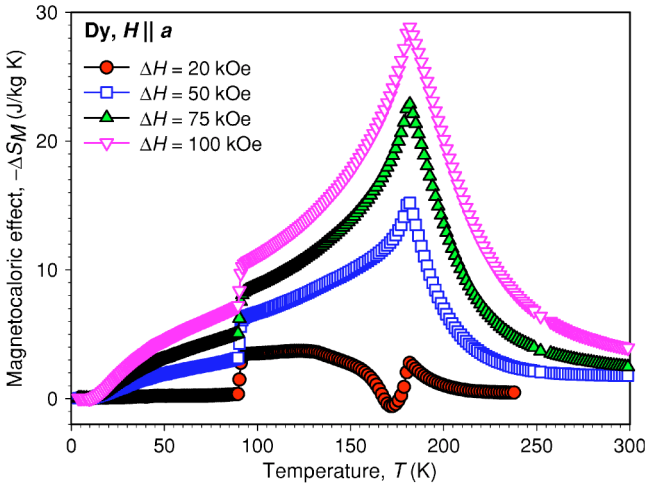

FIG. 23. (Color online) The temperature dependencies of the high-field isothermal magnetic entropy change calculated from the heat capacity in the temperature interval from ~5 to ~300 K.

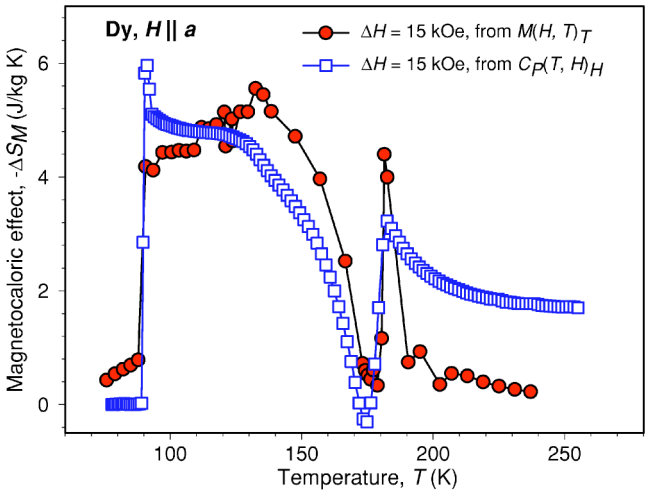

FIG. 24. (Color online) The comparison of the isothermal magnetic entropy change calculated from the heat capacity and the magnetization data for a magnetic-field change of 15 kOe.

agreement with the $\Delta S_{tr}=0.56\pm0.01$ J/mol K at T_C obtained from direct calorimetric measurements of the solid-state electrotransport purified Dy by Pecharsky *et al.*[29] Third, the negative contribution to $|\Delta S_M|$ observed just below T_N in magnetic fields of 20 kOe and lower is consistent with the AFM state of the metal. Finally, between 20 and 50 kOe, there is a large increase in $|\Delta S_M|$ at ~180 K; the magnetic entropy change in the 100 kOe magnetic field reaches the value of $\Delta S_M=-29$ J/kg K at $T=T_N=180$ K, and between ~100 and 300 K the MCE exhibits a typical caretlike behavior in magnetic fields of 50 kOe and higher. All of these features are consistent with the FM state of Dy, which is realized below ~180 K in magnetic fields exceeding 20 kOe.

The isothermal magnetic entropy changes calculated from the heat capacity and magnetization data for a magnetic field change from 0 to 15 kOe with the *a* axis of a crystal parallel to the field are compared in Fig. 24. The agreement is generally good, but above the Néel temperature, the MCE obtained from heat capacity deviates systematically from the MCE calculated from magnetization data. This variance in the $-\Delta S_M$ computed from different experimental data in the paramagnetic region is likely related to the fact that a progressively smaller quantity (ΔS_M) is computed by subtracting progressively larger total entropies. As a result, the relative error in determining ΔS_M from heat capacity rises much faster than the corresponding absolute errors. Similar systematic differences have been noted in the ΔT_{ad} of Gd measured directly and calculated from heat capacity data above the Curie temperature.[44]

In Fig. 25, we compare the magnetocaloric effect measured directly during a magnetic field change from 0 to 10 kOe applied along the *a* axis with the temperature dependencies of the magnetocaloric effect reported earlier.[5,19] In addition to a much sharper rise of the ΔT_{ad} around 90 K, which can be understood because the specimen employed in this study has a higher purity when compared to the crystals used in the past, there is a substantial difference in the MCE's of Dy in the paramagnetic state. The amplitude of the difference is greater than the measurement errors and therefore should not be neglected. Also important is the fact that the greatest deviation from the previous measurements is observed in the immediate vicinity of the Néel temperature, i.e., where short-range correlations, such as AFM clustering, can be significant.

In order to estimate the influence of clustering on the magnetocaloric effect, we first calculate the MCE of Dy assuming the ideal paramagnetic behavior at $T>T_N$. Magnetization, $M(H,T)$, of an ideal paramagnet follows the Curie-Weiss law,

$$M(H,T)=\frac{Np_{eff}^2H}{3k_B(T-\theta_p)}, \tag{32}$$

where N is the number of paramagnetic atoms, k_B is the Boltzmann constant, and θ_p and p_{eff} are 163.5 K and

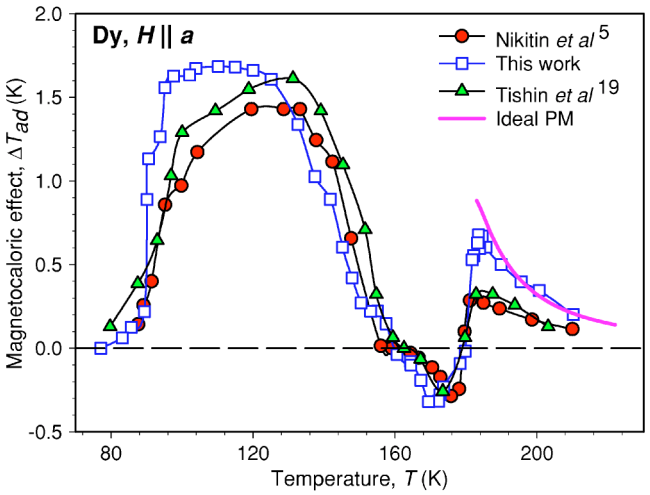

FIG. 25. (Color online) The temperature dependencies of the magnetocaloric effect for a magnetic-field change of 10 kOe in comparison with earlier measurements and the theoretical MCE for Dy assuming an ideal paramagnetic behavior above T_N.

$10.65\mu_B$, respectively. Since the heat capacity of Dy in the paramagnetic state is nearly magnetic-field-independent at 10 kOe and below (see Fig. 8), it can be approximated by the following analytical expression:

$$C(T,H)_{H\leqslant 10\ \mathrm{kOe}} = 220 + \frac{125}{T-180}\ \mathrm{J/kg\ K}. \qquad (33)$$

After substituting Eqs. (32) and (33) into Eq. (24) and integrating, we obtain the following temperature dependence of the MCE above T_N for a magnetic field change $\Delta H = 10$ kOe:

$$\Delta T_{ad}(T)_{\Delta H=10\ \mathrm{kOe}} = -\int_0^{10} \frac{T}{C(T,H)}\frac{dM(T,H)}{dT}dH$$

$$= 2.2\frac{T(T-180)}{(T-179.4)(T-163.5)^2}. \qquad (34)$$

The MCE calculated using Eq. (34) is shown in Fig. 25 as a heavy solid line. The estimated MCE values are in excellent agreement with our experimental data at all temperatures above T_N. The earlier ΔT_{ad} values are smaller than the calculated ones, and the deviations are most obvious in the immediate vicinity of the T_N.

The following qualitative model can be proposed to understand the observed differences. Assuming that AFM clustering can occur at $T > T_N$, Dy may be considered as a paramagnet with a certain amount of embedded AFM phase (AFM clusters) above the T_N. The concentration of these AFM clusters decreases as temperature increases. Naturally, small magnetic field changes produce a negative ΔT_{ad} for an AFM component and a positive MCE for a fraction of the material that is in the PM state. The experimentally measured ΔT_{ad} is the combined total of the two contributions. Therefore, the higher the concentration of the AFM clusters, the lower the observed total MCE and the greater the negative deviation from the ideal paramagnetic behavior. The results shown in Fig. 25 indicate that impurities enhance the AFM clustering in Dy.

The ΔT_{ad} of Dy in strong magnetic fields applied along the *a* axis as calculated from the heat capacity is shown in Fig. 26. The maximum MCE is 19.4 K for the magnetic field change of 100 kOe. Considering both the large values of the isothermal magnetic entropy change (Fig. 23) and the adiabatic temperature change, single crystalline Dy is indeed a promising magnetocaloric material. Its practical use, however, requires that the magnetic field change exceed 2 T in order to eliminate the negative contributions to the MCE due to the presence of the AFM phase.

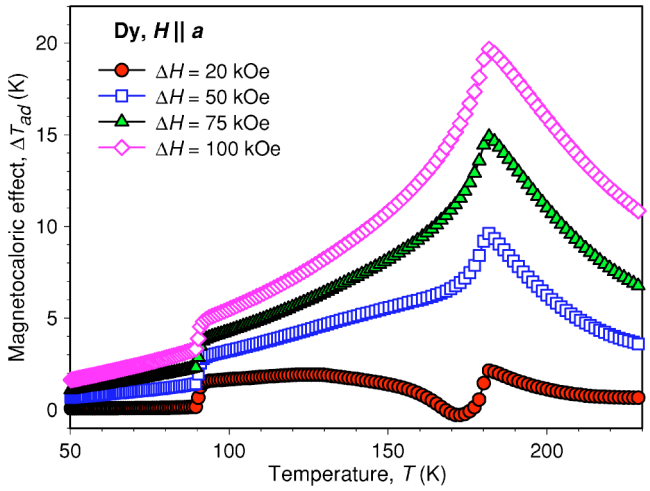

FIG. 26. (Color online) The temperature dependencies of the magnetocaloric effect of Dy as calculated from the heat capacity data.

CONCLUSIONS

As a result of measuring magnetization, ac magnetic susceptibility, heat capacity, and the magnetocaloric effect of single crystals of Dy, we confirmed the majority of previous findings but also report some notable differences in the behaviors of the magnetothermal properties, especially in the vicinities of Curie, Néel, and tricritical temperatures. When the magnetic field vector is parallel to the *a* axis of a crystal, the refined *H-T* phase diagram of Dy is more complicated than previously thought, and it contains several new phases. The appearance of some of these new phases has been explained by considering the Landau-Ginsburg theory of phase transitions.

ACKNOWLEDGMENTS

The authors thank M. I. Ilyn, A. S. Mischenko, Dr. S. Yu. Dan'kov, and Dr. Yu. I. Spichkin for assistance with some of the experimental measurements and useful discussions. Work at Ames Laboratory is supported by the Office of Basic Energy Sciences, Materials Sciences Division of the U. S. Department of Energy, under Contract No. W-7405-ENG-82. Work at Moscow State University is supported by the Russian Foundation for Basic Research under Grant No. 04-02-16709-A.

*Corresponding author. Email address: vitkp@ameslab.gov

[1] J. Jensen and A. R. Mackintosh, *Rare Earth Magnetism: Structure and Excitations* (Clarendon Press, Oxford, 1991).

[2] S. Legvold, in *Ferromagnetic Materials*, edited by E. P. Wohlfarth (North-Holland, Amsterdam, 1980), Vol. 1, Chap. 3, p. 183.

[3] K. A. McEwen, in *Handbook on the Physics and Chemistry of Rare Earths*, edited by K. A. Gschneidner, Jr. and L. Eyring (North-Holland, Amsterdam, 1978), Vol. 1, Chap. 6, p. 411.

[4] R. Hertz and H. Kronmüller, J. Magn. Magn. Mater. **9**, 273

(1978).
[5] S. A. Nikitin, A. S. Andreenko, and V. A. Pronin, Fiz. Tverd. Tela (Leningrad) **21**, 2808 (1979).
[6] V. A. Finkel, *The Structure of Rare Earths* (Metallurgiya, Moscow, 1978).
[7] V. G. Bessergenev, V. V. Gogava, Yu. A. Kovalevskaya, A. G. Mandzhavidze, V. M. Fedorov, and S. I. Shilo, Pis'ma Zh. Eksp. Teor. Fiz. **42**, 412 (1985).
[8] V. G. Bessergenev, V. V. Gogava, A. G. Mandzhavidze, V. M. Fedorov, and S. I. Shilo, Pis'ma Zh. Eksp. Teor. Fiz. **47**, 92 (1988).
[9] V. V. Vorob'ev, M. Ya. Krupotkin, and V. A. Finkel, Sov. Phys. JETP **61**, 1056 (1985).
[10] Y. Kida, K. Tajima, Y. Shinoda, K. Hayashi, and H. Ohsumi, J. Phys. Soc. Jpn. **68**, 650 (1999).
[11] E. B. Amitin, V. G. Bessergenev, and Yu. A. Kovalevskaya, J. Phys. F: Met. Phys. **14**, 2935 (1984).
[12] Y. Shinoda and K. Tajima, J. Phys. Soc. Jpn. **65**, 2367 (1996).
[13] H. U. Astrom and G. Benediktson, J. Phys. F: Met. Phys. **18**, 2113 (1988).
[14] R. D. Greenough, G. N. Blackie, and S. B. Palmer, J. Phys. C **14**, 9 (1981).
[15] R. G. Jordan and E. W. Lee, Proc. Phys. Soc. London **92**, 1074 (1967).
[16] F. Willis and N. Ali, J. Appl. Phys. **69**, 5694 (1991).
[17] F. Willis and N. Ali, J. Appl. Phys. **70**, 6548 (1991).
[18] A. V. Andrianov, Yu. P. Gaidukov, A. N. Vasil'ev, and E. Fawcett, J. Magn. Magn. Mater. **97**, 246 (1991).
[19] A. M. Tishin and O. P. Martynenko, *Physics of Rare Earth Metals in the Vicinity of Magnetic Phase Transitions* (Nauka, Moscow, 1995).
[20] S. W. Zochowski, D. A. Tindall, M. Kahrizi, J. Genossar, and M. O. Steinitz, J. Magn. Magn. Mater. **54-57**, 707 (1986).
[21] J. Dudáš, A. Feher, and Š. Jánoš, J. Less-Common Met. **134**, 9 (1987).
[22] G. I. Kataev, S. V. Red'ko, M. R. Sattarov, and A. M. Tishin, Fiz. Tverd. Tela (Leningrad) **31**, 267 (1989).
[23] W. D. Corner, W. C. Roe, and K. N. L. Taylor, J. Phys. Soc. Jpn. **17**, 1310 (1962).
[24] A. M. Kosevich, V. P. Voronov, and I. V. Manzhos, Zh. Eksp. Teor. Fiz. **2**, 148 (1983).
[25] E. B. Amitin, V. G. Bessergnev, and Yu. A. Kovalevskaya, Zh. Eksp. Teor. Fiz. **84**, 205 (1983).
[26] M. T. Alkhafaji and N. Ali, J. Alloys Compd. **250**, 659 (1997).
[27] S. Yu. Dan'kov, Y. F. Popov, and A. M. Tishin, Vestn. Mosk. Univ., Ser. 3: Fiz., Astron. **35**, 98 (1994).
[28] N. F. Hettiarachi, R. D. Greenough, D. Fort, and D. W. Jones, J. Magn. Magn. Mater. **25**, 310 (1981).
[29] V. K. Pecharsky, K. A. Gschneidner, Jr., and D. Fort, Scr. Mater. **35**, 843 (1996).
[30] K. A. Gschneidner, Jr., V. K. Pecharsky, and D. Fort, Phys. Rev. Lett. **78**, 4281 (1997).
[31] N. Wakabayashi, J. W. Cable, and J. L. Robertson, Physica B **241–243**, 517 (1998).
[32] K. A. Gschneidner, Jr., J. Alloys Compd. **193**, 1 (1993).
[33] V. K. Pecharsky and K. A. Gschneidner, Jr., Adv. Mater. (Weinheim, Ger.) **13**, 683 (2001).
[34] K. A. Gschneidner, Jr. and V. K. Pecharsky, in *Intermetallic Compounds. Principles and Practice*, edited by J. H. Westbrook and R. L. Fleischer (Wiley, New York, 2002), Vol. 3, p. 519.
[35] V. K. Pecharsky, A. P. Holm, K. A. Gschneidner, Jr., and R. Rink, Phys. Rev. Lett. **91**, 197204 (2003).
[36] L. Morellon, Z. Arnold, C. Magen, C. Ritter, O. Prokhnenko, Y. Skorokhod, P. A. Algarabel, M. R. Ibarra, and J. Kamarad, Phys. Rev. Lett. **93**, 137201 (2004).
[37] A. M. Tishin and Y. I. Spichkin, *The Magnetocaloric Effect and Its Applications* (Institute of Physics, Bristol, 2003).
[38] V. K. Pecharsky, J. O. Moorman, and K. A. Gschneidner, Jr., Rev. Sci. Instrum. **68**, 4196 (1997).
[39] V. K. Pecharsky and K. A. Gschneidner, Jr., J. Magn. Magn. Mater. **200**, 44 (1999).
[40] B. Coqblin, *The Electronic Structure of Rare-Earth Metals and Alloys: The Magnetic Heavy Rare-Earths* (Academic, London, 1977).
[41] Yu. A. Izyumov, Usp. Fiz. Nauk **144**, 493 (1984).
[42] Yu. A. Izyumov and V. M. Laptev, Zh. Eksp. Teor. Fiz. **143**, 2185 (1983).
[43] V. K. Pecharsky, K. A. Gschneidner, Jr., A. O. Pecharsky, and A. M. Tishin, Phys. Rev. B **64**, 144406 (2001).
[44] S. Yu. Dan'kov, A. M. Tishin, V. K. Pecharsky, and K. A. Gschneidner, Jr., Phys. Rev. B **57**, 3478 (1998).